International Journal of Multiphase Flow 142 (2021) 103709

Contents lists available at ScienceDirect

International Journal of Multiphase Flow

journal homepage: www.elsevier.com/locate/ijmulflow

An engineering stability technique for unsteady, two-phase flows with heat and mass transfer

Faith R. Beck[a,*], Lokanath Mohanta[a,b], Diane M. Henderson[c], Fan-Bill Cheung[d,e], Gita Talmage[d]

[a] Work performed at the Department of Mechanical Engineering, The Pennsylvania State University, University Park, PA 16802, USA
[b] Carrier Corporation, Syracuse, NY 13221, USA
[c] Department of Mathematics, The Pennsylvania State University, University Park, PA 16802, USA
[d] Department of Mechanical Engineering, The Pennsylvania State University, University Park, PA 16802, USA
[e] Department of Nuclear Engineering, The Pennsylvania State University, University Park, PA 16802, USA

ARTICLE INFO

Article history:
Received 22 November 2020
Revised 19 April 2021
Accepted 28 May 2021
Available online 31 May 2021

Keywords:
Two-phase flow
Stability
Oscillations
Heat and mass transfer

ABSTRACT

This paper considers the stability of an unsteady, two-phase flow with heat and mass transfer. The model problem is motivated by loss of coolant accidents in nuclear power plants. For the example problem, two flow geometries are considered: inverted annular flow boiling and an annular mist flow. The model is comprised of coupled Mathieu equations so that stability can be determined using a Floquet analysis. The flow is found to be mathematically unstable to all perturbative wavenumbers, but for practical purposes there are regions of stability. Using the solution's growth behavior and doubling-time, the notion of practical stability, which is termed herein as "engineering stability," is quantified and a method is provided for application to other engineering stability problems.

1. Introduction

This paper proposes a technique to determine the engineering stability for unsteady, or oscillatory flows. Oscillating flows present unique effects on turbulent intensities (Sleath, 1987) and diffusion (Watson, 1983), which have application to both the man-made and natural world. Flow oscillations and their impacts are of interest for oceanic studies (Lowe et al., 2005), power generation (Bestion, 2004), and chemical processes (Harvey et al., 2001).

Time varying, and in particular, oscillating flows are often unstable, but with small growth rates as compared to some time period of interest (Razavi et al., 2016; Kelly, 1965). Their mathematical stability can be determined using Floquet theory, which is one method for solving linear ordinary differential equations whose coefficients and/or boundary conditions are periodic (Coddington and Levinson, 1955). For example, Benjamin and Ursell (1954) studied the stability of the free surface of an inviscid fluid in a circular cylinder undergoing periodic vertical motion, such that the system is parametrically forced due to a time-varying acceleration of gravity. From Benjamin and Ursell (1954), a stability analysis at the free surface leads to a Mathieu equation, so that there are regions of instability to perturbations whose resonance frequencies are harmonics of the parametric forcing frequency. In these regions of instability, the free surface exhibits standing waves that oscillate at the resonant frequency, with amplitudes that will grow until nonlinear effects become significant (Drazin and Reid, 2004). This system is often referred to as “Faraday waves” (Faraday, 1837) and has been the subject of many analytic, numerical, and experimental studies.

There have been generalizations by, for example, Kumar (1996), who allowed for viscous effects, and Kumar and Tuckerman (1994), who considered the stability of an interface between two fluids undergoing vertical oscillations. Such parametric excitations occur in other systems, for example, vibrated, wetting liquid drops supported by a solid plate (Maksymov and Pototsky, 2019), floating drops with deformable domains (Pucci, 2015), and multi-frequency parametric forcing in smallest chemical reactions (Zhou et al., 2020).

In particular, Kelly (1965) investigated the stability of an unsteady Kelvin–Helmholtz flow with surface tension. The effect of viscous stresses not included, Kelly found that the interface between two inviscid fluids became unstable due to periodic perturbations. More recently, Razavi et al. (2016) studied the stability of a system modeled by coupled Hill’s equations using Floquet theory. *They identified regions of stability, even though perturbations in these regions had positive growth rates*. Floquet theory defines sta-

* Corresponding author.
E-mail address: faith.r.beck@gmail.com (F.R. Beck)

bility in terms of eigenvalues, λ_i, which provide the growth rates of the perturbations, such that if $|\lambda_i|,\ (i = 1, 2, \ldots, n)$, are all less than one, then the system is mathematically stable. In the system studied by Razavi et al. (2016), the largest $|\lambda_i|$ was close to one, but greater than one, so the perturbations would grow, but slowly. The idea that $|\lambda_i| \gtrsim 1$ may be considered stable for engineering purposes, is the focus of this paper.

Here, we pursue this idea further, and quantify it using a model unsteady flow problem motivated by a loss of coolant accident (LOCA). To this end, we define "engineering stability." Engineering stability is determined by the amount of growth of perturbations during the operational period, whereas mathematical stability is determined by non-positive growth rates. Instead of focusing on whether $|\lambda_i| < 1$, engineering stability is concerned with the rate of perturbation growth over a time period that is of physical relevance, and what the consequences of that amount of growth are on the physical system. For a particular physical system, one can determine the tolerance for perturbation growth during the time that the system is operational. Then the question of engineering stability becomes: how large can the eigenvalues be such that the perturbation growth is bounded by the desired tolerance?

In this paper, we show that the value for $\lambda_{\max}$ is determined such that the tolerance for perturbation growth is a factor of two, and the time for the perturbation to double in size (i.e. the doubling-time) is within the operational period of the system. If it is, then we consider the system to be unstable from an engineering perspective. In particular, a system of equations with time-varying, periodic coefficients, whose solution is v_i, can be represented at a later time $(t + nT)$, for example by Nayfeh and Mook (2008) as

$$v_i(t + nT) = \lambda_i^n v_i(t), \tag{1.1}$$

where t is time, n is the number of oscillation periods, and T is the oscillation period. Herein, we consider the system to have engineering stability if all values of λ_i are such that $v_i(\mathcal{T}) \leq 2v_i(0)$, where $\mathcal{T}$ is the time period over which the system is operational.

A growth factor of e, rather than two, and its corresponding e-folding time, is another common choice. For example, an e-folding time is used in oceanography, biology, and cosmology to understand the propagation of instabilities with time (Stone, 1972; Rumfeldt et al., 2008; Pitari et al., 2016). While e-folding time has been used to measure perturbation growth for other applications, this is the first time, to the best of the authors' knowledge, that such parameters have been used as a stability criterion. We note that a factor of two is the more conservative choice than a factor of e, and has relevance for the system considered (see discussion in Section 4). The physical example used herein includes heat and mass transfer, viscous effects at the interface, and a time-varying flow velocity. This applied method for stability provides an additional, simple metric with which to analyze a complex, two-phase system.

2. Example problem

The model problem is motivated by applications to nuclear power plants in which there is oscillatory flooding of a heated tube. Perturbations that have large enough growth rates could worsen nuclear power accidents, more specifically during a LOCA. We define the flow in Section 2.1, establish the initial and boundary conditions, and determine the coupled Mathieu equations that will be used for the stability analyses in Section 2.2.

2.1. Flow description

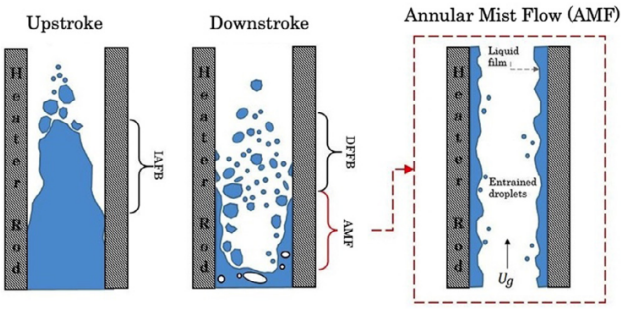

Fig. 1. Prominent flow regimes during an up- and downstroke (Beck, 2019).

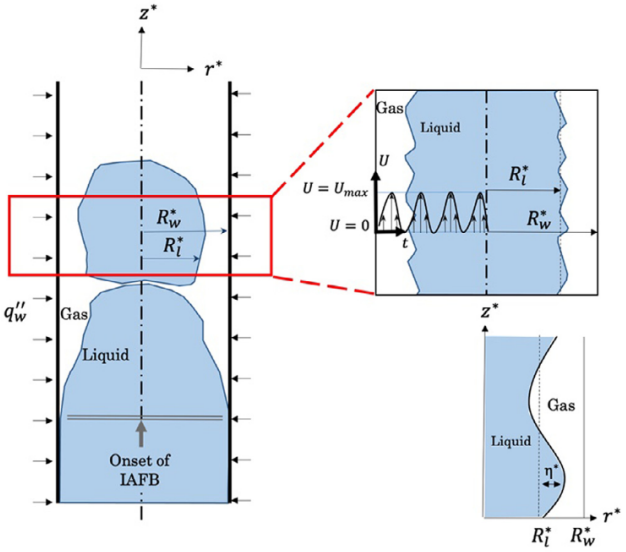

Fig. 2. Approximating IAFB geometry during an upstroke as an annulus with liquid at the center and gas on the walls (Beck, 2019).

oscillatory flooding of a heated tube, Oh et al. (1986) found that the void fraction, or fraction of the flow channel volume that is occupied by gas, and hence the flow regimes, oscillate between Inverted Annular Flow Boiling (IAFB) and Annular Mist Flow (AMF), as illustrated in Fig. 1. Here, the IAFB geometry is depicted during an upstroke. Slugs and droplets of liquid are sheared from the incoming jet by fast moving vapor downstream. In contrast, during a downstroke, AMF is present with dispersed flow film boiling (DFFB) occurring further downstream. Together, Fig. 1 shows the downstream effects of different flow regimes present in an oscillating flow.

During an upstroke, the high velocity liquid jet cannot come in direct contact with the heated wall due to high temperature vaporization there, and resembles IAFB. The IAFB geometry can be approximated as an annulus with liquid in the center and gas on the walls, shown in Fig. 2. By contrast, for low flooding rates or during a downstroke, AMF occurs, with gas in the center and liquid along the walls. The AMF geometry is simply the inverse of Fig. 2. Since both flow geometries are required to characterize oscillatory flow, stability analyses are performed on both the IAFB and AMF geometries in the following sections. However, for brevity, the IAFB geometry will be used as an example for the majority of the provided equations. Identical assumptions and approximations are

assumed incompressible due to its low velocity, which for this example has a Mach number < 0.3. Specific to this problem, nuclei production is not a dominant mechanism for interfacial instabilities. Since the bulk liquid is significantly subcooled (between 22 to 55 K), when vapor bubbles are generated on the heated surface for the AMF geometry, they will instantaneously collapse as they depart. Additionally, for the IAFB geometry, since the gas phase, rather than the liquid, is in direct contact with the heated surface, there will be no nucleation for this flow type. Therefore, for the two flow geometries, nuclei production is not considered a dominant mechanism for instability.

Additionally, since the gas and liquid layers are so thin along the wall (see Fig. 2) variations in r will be insignificant, so $\frac{\partial}{\partial r} \approx 0$ in the film. From Fig. 2, q''_w is the wall heat flux, R^*_w is the dimensional, radial distance from the center of the annulus to the wall, R^*_l is the dimensional, radial distance from the center of the annulus to the edge of the liquid core, η^* is the dimensional height of the interfacial wave, and $U(t)$ represents the oscillating velocity of the liquid and gas phases.

We note that since the flows are incompressible and irrotational, viscous-potential flow theory (Funada and Joseph, 2001) is used, which assumes that the viscosity is only significant at the interface between the two fluids. Therefore, viscous forces do enter the analysis through the normal stress balance at the interface between the liquid and gas. This approximation is reasonable in wave motions where the viscous resistance to these waves is not negligible, or when the gas phase shear stress is sufficiently small. While gas phase turbulence and the consequential liquid entrainment that occurs would be present in a real flow, to keep the analysis linear, these effects are neglected herein. The following analysis is provided in full detail in Beck (2019) and Mohanta et al. (2016). However, for the work by Mohanta et al. (2016), the flow is steady, as opposed to the unsteady flows presented here.

In the following equations, $()^*$ denotes dimensional quantities and terms without an asterisk are non-dimensional. Additionally, because the method of normal modes will be used, terms with a $()_0$ refer to the base (or unperturbed) state of the oscillatory flow for either the liquid or gas phase, and ω refers to the oscillation frequency of the base flow. The flow will be considered in terms of an undisturbed base flow and a small perturbation to the base flow. The base states of the liquid (l) and gas (g) are oscillating, with velocity potentials ($\phi^*_{i,0}$), where $i = (l, g)$ as

$$\phi^*_{i,0} = U^*_{i,0} \sin(\omega^* t^*). \tag{2.1}$$

The velocity of each phase $U^*_{i,0}$ is defined as

$$U^*_{i,0} = \frac{\dot{m}^*_i}{\rho^*_i A^*_i}. \tag{2.2}$$

In (2.1) and (2.2), ω^* is the base flow oscillation frequency, U^*_i is the base flow velocity, ρ^*_i is the density, A^*_i is the flow area, $\dot{m}^*_i$ is the average mass flow rate, and t^* is time. Since the base flow is irrotational, velocity potentials are found by solving Laplace's equation in the liquid and gas so that

$$\nabla^{*2} \phi^*_{i,0} = 0. \tag{2.3}$$

With the axisymmetric flow assumption, the Laplacian operator is

$$\nabla^{*2} = \frac{\partial^2}{\partial r^{*2}} + \frac{1}{r^*}\frac{\partial}{\partial r^*} + \frac{\partial^2}{\partial z^{*2}}. \tag{2.4}$$

The Bernoulli equation is used to determine the pressures in both the liquid and gas phases. For irrotational flows, the unsteady

$$\frac{\partial \phi^*_{g,0}}{\partial t} + \frac{1}{2}(\nabla^* \phi^*_{g,0}) \cdot (\nabla^* \phi^*_{g,0}) + \frac{p^*_{g,0}}{\rho^*_g} + g^* z^* = H^*_2(t^*), \tag{2.6}$$

where $H^*_1(t)$ and $H^*_2(t)$ represent time-dependent coefficients that are determined using the velocity potentials and the Young–Laplace equation (Panton, 2013). The Young–Laplace equation relates the pressures of both phases, the surface tension (σ^*), and surface curvature of the undisturbed liquid at the interface (κ^*_0) as

$$p^*_{l,0} - p^*_{g,0} = \sigma^* \kappa^*_0. \tag{2.7}$$

Eqs. (2.1) - (2.7) represent the base states for flows in both geometries, IAFB and AMF. The scales used to non-dimensionalize variables for the IAFB geometry are

$$[\text{length, velocity, time, pressure}] = \left[2R^*_l, U^*_{g,0}, \frac{2R^*_l}{U^*_{g,0}}, \rho^*_g U^{*2}_{g,0}\right]. \tag{2.8}$$

The quantity $2R^*_l$ is selected as the length scale for the IAFB geometry because it simplifies the non-dimensionalization of the interface. The resulting non-dimensional lengths, time, and pressure for the IAFB geometry are

$$[z, r, t, p] = \left[\frac{z^*}{2R^*_l}, \frac{r^*}{2R^*_l}, \frac{t^* U^*_{g,0}}{2R^*_l}, \frac{p^*}{\rho^*_g U^{*2}_{g,0}}\right]. \tag{2.9}$$

The AMF geometry uses the same non-dimensionalizations except for the length scale, which is chosen as $2R^*_g$, the radius of the gas phase.

The ratios of base flow velocity, density, and dynamic viscosity are

$$\psi = \frac{U^*_{l,0}(t)}{U^*_{g,0}(t)}, \tag{2.10a}$$

$$\gamma = \frac{\rho^*_g}{\rho^*_l}, \tag{2.10b}$$

$$\zeta = \frac{\mu^*_g}{\mu^*_l}. \tag{2.10c}$$

In this problem, four dimensionless parameters arise: gas Reynolds (Re_g), gas Weber (We_g), Froude (Fr), and Strouhal (St) numbers that are defined as

$$Re_g = \frac{U^*_{g,0} 2R^*_l}{\nu^*_g}, \tag{2.11a}$$

$$We_g = \frac{\rho^*_g U^{*2}_{g,0} 2R^*_l}{\sigma^*}, \tag{2.11b}$$

$$Fr = \frac{U^{*2}_{g,0}}{\omega^* \cdot 2R^*_l}, \tag{2.11c}$$

and

$$St = \frac{\omega^* 2R^*_l}{U^*_{g,0}}. \tag{2.11d}$$

To evaluate the stability of the system, perturbations are applied to the total velocity, pressure, and velocity potentials as

$$\tilde{u}_i = U_{i,0} + u_i, \tag{2.12}$$

$$\tilde{p}_i = P_{i,0} + p_i, \tag{2.13}$$

Table 1
Boundary conditions for both flow geometries.

	At $r = 0$	At $r = r_w$
IAFB	$U_{l,r}\|_{r=0} = \frac{\partial \phi_l}{\partial r}\|_{r=0} < \infty$	$\frac{\partial \phi_g}{\partial r}=0$
AMF	$U_{g,r}\|_{r=0} = \frac{\partial \phi_g}{\partial r}\|_{r=0} < \infty$	$\frac{\partial \phi_l}{\partial r}=0$

2.2. Boundary conditions and governing equations

A total of five conditions are needed to evaluate the two-fluid, coupled system in two-dimensions. Conditions include one no-flow boundary condition at the wall ($r = r_w$), one finite solution condition along the centerline ($r = 0$), and three interfacial conditions derived from conservation of mass, momentum, and energy. The three interfacial conditions will be defined in this section.

The two conditions at $r = 0$ and $r = r_w$ are functions of the flow geometry and are listed in Table 1. The dimensional perturbed interface equation for the IAFB geometry is

$$F^*(r^*, z^*, t^*) = r^* - R_l^* - \eta^*(z^*, t^*), \tag{2.15}$$

and for the AMF geometry, the dimensional perturbed interface is

$$F^*(r^*, z^*, t^*) = r^* - R_g^* - \eta^*(z^*, t^*), \tag{2.16}$$

where η^* represents the location of the liquid-gas interface, r^* a radial position, and R_l^* and R_g^* the dimensional radii of the liquid and gas phases, respectively. The relationship for the non-dimensional interface between the two fluids for the IAFB and AMF geometries is the same. The simplified, non-dimensional Eq. (2.17) for the free surface is the reason for choosing the scales provided in (2.8) and (2.9):

$$F(r, z, t) = r - \frac{1}{2} - \eta(z, t). \tag{2.17}$$

The method of normal modes is applied to the velocity potentials at the interface location, of the form

$$\left[\phi_l(r, z, t), \phi_g(r, z, t), \eta(z, t)\right] = \left[\hat{\phi}_l(r, t), \hat{\phi}_g(r, t), \hat{\eta}(t)\right] e^{ikz}. \tag{2.18}$$

Performing mass, momentum, and energy balances at the two-phase interface between the liquid and gas yields the final governing equations in terms of the unknowns $A(t)$, $C(t)$, $\hat{\eta}(t)$, and their derivatives, where A and C are two unknowns originating from the independent eigenfunctions of (2.3). The mass, momentum, and energy balances at the linearized interface, $r = \frac{1}{2}$, respectively are

$$\frac{1}{\gamma}\frac{d\hat{\eta}}{dt} = -A(t)a_1 k + C(t)k\left\{\frac{1}{\gamma} + I_1\left(\frac{k}{2}\right)k\right\} + \hat{\eta}(t)ik\left[1 - \sin(St \cdot t)\right]\left\{1 - \frac{\psi}{\gamma}\right\} = 0, \tag{2.19}$$

$$\frac{1}{\gamma}\frac{dC(t)}{dt} I_0\left(\frac{k}{2}\right) - \frac{dA(t)}{dt}a_0 = -C(t)\left\{\frac{\psi}{\gamma}[1 - \sin(St \cdot t)]\right.$$
$$\left. ikI_0\left(\frac{k}{2}\right) + \frac{2}{Re_g\zeta}\frac{k^2}{2}a_2\right\} - A(t)\left\{[1 - \sin(St \cdot t)]ika_0 + \frac{2}{Re_g}\frac{k^2}{2}(a_2 + a_3)\right\} + \hat{\eta}(t)\left\{\frac{4 - k^2}{We_g}\right\}, \tag{2.20}$$

and,

where I_j is a modified Bessel function of the first kind.

The system of Eqs. (2.19)–(2.21) will lead to a singular matrix. To avoid this, we manipulate (2.19) and (2.21) by solving for $\frac{d\hat{\eta}(t)}{dt}$ in (2.19), substituting into (2.21), and then taking the derivative with respect to time, yielding

$$\frac{dC(t)}{dt}kI_1\frac{k}{2} - \frac{dA(t)}{dt}a_1 + \frac{d\hat{\eta}(t)}{dt}\left\{\Lambda S'(0)\left[\frac{1}{\gamma} - 1\right] + ik[1 - \sin(St \cdot t)][1 - \psi]\right\} = \hat{\eta}(t)\left\{ik(1 - \psi)[\cos(St \cdot t)]St\right\}. \tag{2.22}$$

Here, Eq. (2.22) is a modified form of conservation of energy that leads to a diagonalizable system of equations to be analyzed using Floquet theory.

Only the final governing equations for the IAFB geometry are provided here. We choose to use Eqs. (2.19), (2.20), and (2.22); however, if (2.20), (2.21), and (2.22) were used instead, the results would be the same. For a complete derivation of the governing equations for both flow geometries, see Beck (2019). These equations are used to determine the fundamental set of solutions required for the method of normal modes to analyze the stability.

For (2.19)–(2.22), coefficients a_i, where $i = (0,1,2,3)$ are given as

$$a_0 = I_0\frac{I_1(k_{r_w})}{K_1(k_{r_w})}K_0\left(\frac{k}{2}\right), \tag{2.23a}$$

$$a_1 = k\left[I_1\left(\frac{k}{2}\right) - \frac{I_1(k_{r_w})}{K_1(k_{r_w})}K_1\left(\frac{k}{2}\right)\right], \tag{2.23b}$$

$$a_2 = I_0\left(\frac{k}{2}\right) + I_2\left(\frac{k}{2}\right), \tag{2.23c}$$

$$a_3 = \left[K_0\left(\frac{k}{2}\right) + K_2\left(\frac{k}{2}\right)\right]\left[\frac{I_0(k_{r_w})}{I_1(k_{r_w})}\right], \tag{2.23d}$$

where K_j is a modified Bessel function of the second kind.

3. Determination of mathematical stability for an unsteady flow

3.1. Numerical analysis

Since the coefficients of the ordinary differential equations are periodic functions of time, Floquet theory can be used to solve the governing equations with oscillating velocities. The three equations for the three unknowns are conservation of mass (2.19), momentum (2.20), and modified conservation of energy (2.22), which are assembled as

$$\mathbf{Q_1}(t)\begin{bmatrix}\frac{dA(t)}{dt}\\ \frac{dC(t)}{dt}\\ \frac{d\hat{\eta}(t)}{dt}\end{bmatrix} = \mathbf{Q_2}(t)\begin{bmatrix}A(t)\\ C(t)\\ \hat{\eta}(t)\end{bmatrix}, \tag{3.1}$$

where $\mathbf{Q_1}(t)$ and $\mathbf{Q_2}(t)$ are both 3×3 matrices, and $Q_i(t) = Q_i(t + T)$, $(i = 1, 2)$, are time-dependant, periodic coefficients.

To solve this system of equations, (3.1) is rewritten as

$$\begin{bmatrix}\frac{dA(t)}{dt}\\ \frac{dC(t)}{dt}\\ \frac{d\hat{\eta}(t)}{dt}\end{bmatrix} = \mathbf{Q_1}(t)^{-1}\mathbf{Q_2}(t)\begin{bmatrix}A(t)\\ C(t)\\ \hat{\eta}(t)\end{bmatrix}. \tag{3.2}$$

Our choice of the modified conservation of energy Eq. (2.22) guar-

Table 2
Parameters for stability analyses.

	α	T_w (K)	Re_g	We_g
IAFB	0.9	600	4000	24
AMF	0.99	404	20,200	76

The eigenvalues of the solution vector, **F**, determine the stability of the system (Nayfeh and Mook, 2008). The eigenvalues are established by solving

$$\begin{bmatrix} f_{11}-\lambda_1 & 0 & 0 \\ 0 & f_{22}-\lambda_2 & 0 \\ 0 & 0 & f_{33}-\lambda_3 \end{bmatrix} = 0. \tag{3.3}$$

Because of the periodicity of the coefficients, the solution vector, $\mathbf{F}(t)$, at any time $t = nT$, $(n = 0, 1, \ldots)$, will be proportional to $(\mathbf{F}(T))^n$. Thus, one can show that if the three moduli of eigenvalues $[|\lambda_1|, |\lambda_2|, |\lambda_3|]$ are all less than one, then the system is considered stable. The following method is used to evaluate the stability of the system of equations:

(i) A range of wavenumbers (k) and Strouhal numbers (St) is chosen to evaluate the temporal stability and swept in two loops. Values of St, ranging from 10^{-5} to 10^{-2}, are selected based on experiments by Beck (2019), which have oscillation frequencies varying from two to 10 s.
(ii) An initial condition vector is specified, $[x_0]$, which includes the initial values for $A(t)$, $C(t)$, and $\hat{\eta}(t)$, respectively, at $t = 0$.
(iii) The system of equations is integrated from 0 to $\frac{2\pi}{St(i)}$, where (i) is the vector that contains the range of St values. The range for the period of integration is chosen to ensure that one full oscillation period is evaluated, where $T = \frac{2\pi}{St(i)}$. Each coefficient is checked to confirm that the largest full period is used.
(iv) The relative and absolute tolerances to perform the integrations are set to 10^{-7}. Smaller tolerances were tested with no significant effect on the results.
(v) For every combination of k and St, the eigenvalues are calculated.
Based on the eigenvalues, stability is determined using

$$\lambda_{\max} = \max\left(|\lambda_1|,\ |\lambda_2|,\ |\lambda_3|\right) < 1. \tag{3.4}$$

If (3.4) is satisfied, then the base flow is mathematically stable.
(vi) If (3.4) is not satisfied, then we consider the possibility of engineering stability (see Section 4).

3.2. Parametric study

The combined effects of void fraction (α), temperature of the heated wall (T_w), Re_g, and We_g on the stability of both flow geometries are discussed here. For individual parameter effects, see Beck (2019). Table 2 shows the parameters used to determine the mathematical stability provided in Figs. 3 and 4. The conditions listed in Table 2 are based on experimental data from Beck (2019), with approximate values:

(i) $U_g \approx$15 m/s,
(ii) U_l between 0.0254 to 0.1524 m/s,
(iii) oscillation period between two and 10 s,
(iv) system pressure between 138 to 414 kPa,
(v) liquid temperature between 22 to 55 K subcooled,
(vi) and a vapor temperature above saturation.

Figs. 3 and 4 show maximum eigenvalues for the IAFB and AMF

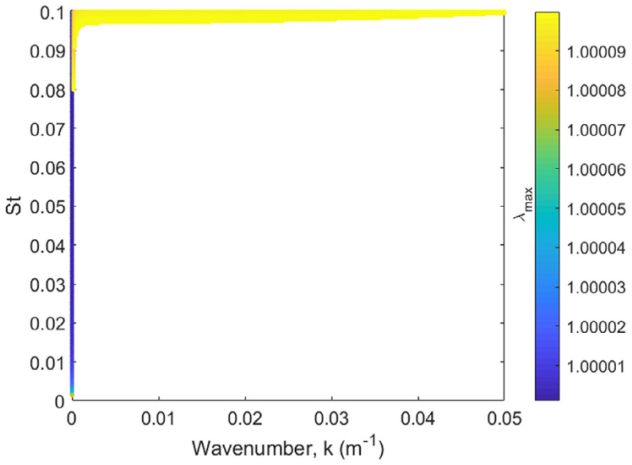

Fig. 3. Maximum eigenvalues for the IAFB geometry resulting from (3.4).

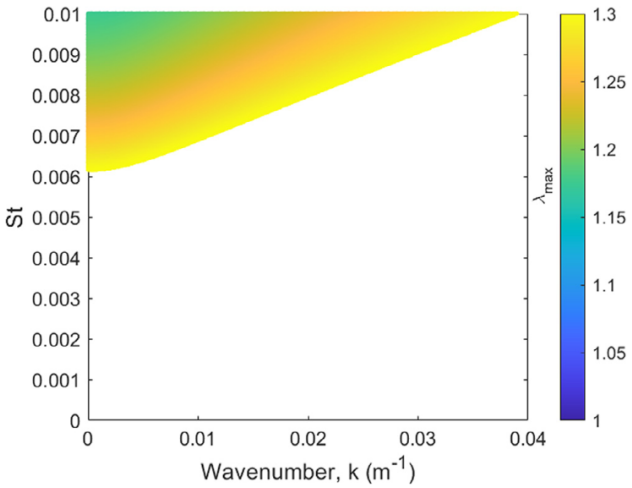

Fig. 4. Maximum eigenvalues for the AMF geometry resulting from (3.4).

without color, represented with white, include eigenvalues that are larger than the maximum color-bar value.

In Fig. 3, the IAFB geometry with combined effects of Re_g, We_g, St, and heat transfer effects, has a minimum eigenvalue $\lambda = 1.0000001$, which is greater than one. Additionally, Fig. 4 shows the AMF geometry with the same combined effects and has a minimum eigenvalue $\lambda = 1.175$. While dimensionless parameters Re_g and We_g have little effect on the stable regions, the addition of heat transfer significantly reduces the stability of the system. In a full parametric study by Beck (2019), it was determined that the addition of heat transfer at the interface primarily reduces the stability of the system.

Heat transfer promotes instabilities, as reported in the literature, specifically for the AMF configuration (Nayak and Chakraborty, 1984; Beck, 2019). For the AMF geometry, the thin liquid film between the heated wall and the gas will be close to, or near, its saturation temperature. In this state, the liquid requires minimal additional heat to initiate vaporization there, and this leads to an instability. This result is similar to what is observed by Nayak and Chakraborty (1984), where the addition of

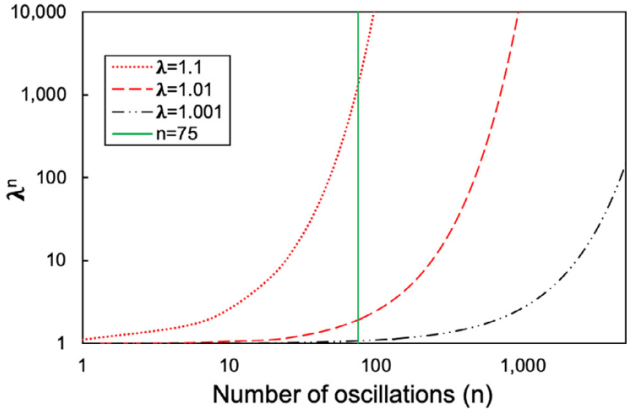

Fig. 5. Different λ_{max} solutions as functions of number of oscillations. The green vertical line at $n = 75$ oscillations denotes the duration of oscillations for the example problem.

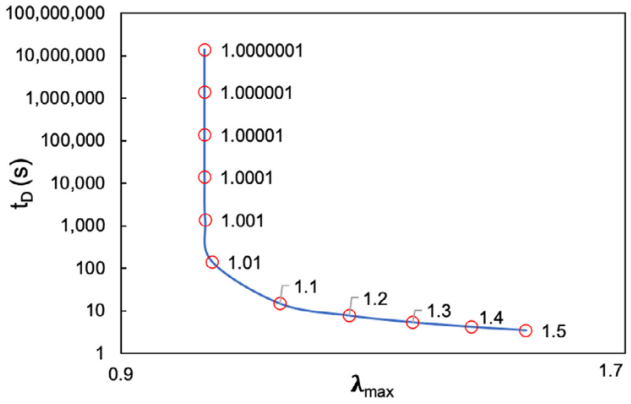

Fig. 6. Doubling-time depicted for each λ_{max} solution.

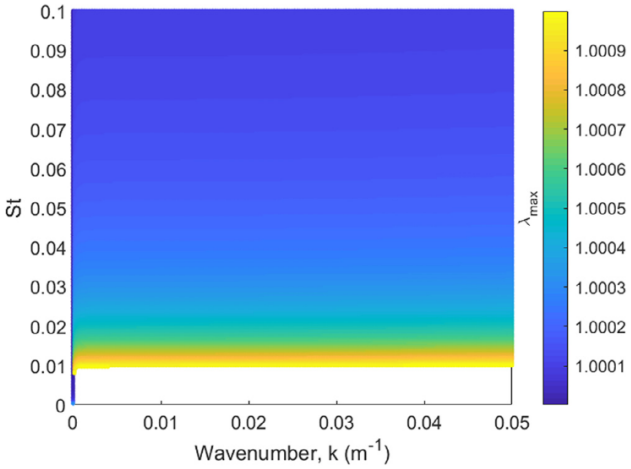

Fig. 7. Extended maximum eigenvalues for the IAFB geometry based on engineering stability criteria, $\lambda_{max} < 1.001$.

flow increases the amount of liquid carryover compared to constant flow. The amount of liquid carryover, or entrained liquid in the carrier gas phase, can be used to physically quantify the effects of the interfacial instability, for when the interface becomes unstable, liquid break-up will occur.

Since both flows (IAFB and AMF) are mathematically unstable ($\lambda > 1$) in the range of Strouhal number and wavenumbers of interest, this suggests that the flows are unstable given realistic conditions in an experiment or nuclear reactor undergoing flow boiling. However, we make the case that these flows can be described as "engineering stable," for eigenvalues that are $\lambda = 1 + \epsilon$, where $\epsilon \ll 1$.

In Section 4, we describe how flow oscillations observed during a finite time period can be used to predict solution growth during that time. The example problem will be used to define an engineering stability criterion for this flow and demonstrate how engineering stability may be determined for other flows.

4. Determining engineering stability

Engineering stability is unique for each application, since the limits for λ_{max} are problem-specific. To determine engineering stability, perturbation growth rate and doubling-time are evaluated. Together, this information will be used to characterize the engineering stability criterion for the example problem.

Fig. 5 depicts three different eigenvalues with predicted perturbation growth in time, using (1.1). It shows that when $\lambda^n \leq 1.001$, the perturbation amplitude does not double before the time of interest, shown as 75 oscillations in the figure. The time of interest is chosen as 75 oscillations, or 150 s with a two second oscillation period, because flow oscillations during a LOCA are most prominent within this time-frame (Beck, 2019; Beck et al., 2016, 2018; Bestion, 2004; Cheung et al., 2014). In contrast, for those eigenvalues greater than 1.001, the perturbation growth tends to increase by orders of magnitude within the first 10 oscillations.

The solution's doubling-time can provide an additional metric for defining engineering stability. The doubling-time refers to the time it takes for a solution to double in magnitude, or

$$t_D = \frac{T\ ln(2)}{ln(|(\lambda_{max}|)}, \tag{4.1}$$

Perturbation growth for this example is allowed as long as the perturbation amplitude does not approach the radius, R, which can either be defined as $R = (R_w - R_l)$ for the IAFB geometry or $R = (R_w - R_g)$ for the AMF geometry. To use t_D as a representative timescale for solution growth, we can write this criterion in terms of the wavelength, L_f, and the radius R, such that

$$\frac{0.2L_f}{2\pi R} < 1. \tag{4.2}$$

If (4.2) is satisfied, then the doubling-time can be used as a representative timescale for the example problem's solution growth. As an example, the IAFB geometry's oscillation velocity and frequency determine L_f to be 50.8 mm. Together, the wavelength with $R = 1.9$ mm, satisfies (4.2) since $0.85 < 1$.

A large doubling-time, compared to the operational time, suggests that the perturbation amplitude will not significantly increase within the operational time of interest, which for this example is 150 s. Fig. 6 shows that for $\lambda_{max} < 1.001$, the doubling-time of the solution is sufficiently small compared to the operational time. Both Figs. 5 and 6 suggest that the system with eigenvalues < 1.001 can be considered "stable" for engineering purposes in this example. For this application, we can extend the stability criterion from $\lambda_{max} < 1$ to $\lambda_{max} < 1.001$.

Fig. 7 shows engineering stability for the IAFB geometry, whose

engineering sense. Therefore, with engineering stability, it is shown that the IAFB geometry can be considered stable for particular *St* and experimental conditions, whereas the AMF geometry is unstable for the same conditions with Re_g, and We_g, and heat transfer effects. Since the AMF geometry is not continuously present during a LOCA, the flow system is capable of reaching stable conditions.

5. Summary and conclusions

In this paper, mathematical and engineering stability are compared using an unsteady two-phase flow with heat and mass transfer. Determining the engineering stability is particularly useful when the given problem is mathematically unstable, but with "slow enough" growth rates, as in the presented example. For this problem, engineering stability is used to extend the limits on stability for practical purposes. Although the application and analyses presented here are specific to this flow, the method for determining engineering stability can be extended to other types of problems. To do so, the following should be considered:

(i) an operational time period for which the system is running,
(ii) a tolerance for perturbation growth, and
(iii) values of λ_{max} over ranges of physical parameters of interest, for which the doubling-times are less than the operational times.

After evaluating the growth rates and doubling-times, a cut-off for λ_{max} can be established, beyond which the perturbation will increase above the allowed tolerance within the operational time period and be considered unstable in an engineering sense.

For the example problem described in the text, the following conclusions were made after determining the engineering stability criterion particular to this problem.

(i) For the AMF geometry, the addition of heat and mass transfer significantly decreased the stability of the system.
(ii) Using a problem-specific time-scale for solution growth, $\lambda_{max} < 1$ can be extended to $\lambda_{max} < 1.001$.
(iii) For the IAFB geometry, engineering stability extended the range of meaningful solutions for applied stability.

While both the tolerance for perturbation growth and the operational time period will be unique for each problem, computing the engineering stability can extend the range of meaningful solutions for a better physical understanding of the flow.

Declaration of Competing Interest

The authors declare that they have no known competing financial interests or personal relationships that could have appeared to influence the work reported in this paper.

CRediT authorship contribution statement

Faith R. Beck: Writing - original draft, Writing - review & editing, Conceptualization, Methodology. **Lokanath Mohanta:** Formal analysis, Writing - review & editing. **Diane M. Henderson:** Formal analysis, Writing - review & editing, Conceptualization, Methodology. **Fan-Bill Cheung:** Supervision, Writing - review & editing. **Gita Talmage:** Formal analysis, Writing - review & editing, Methodology.

Acknowledgments

Pratim Mishra for his suggestions with the numerical simulations in this paper.

References

Beck, F.R., 2019. Experimental and Theoretical Study of Oscillatory Two-Phase Flows with Heat and Mass Transfer Ph.D. thesis.
Beck, F.R., Jin, Y., Cheung, F.B., Bajorek, S.M., Tien, K., Hoxie, C.L., 2018. A study of liquid entrainment in oscillatory flows. Embedded Topical International Meeting on Advances in Thermal Hydraulics (ATH 2018), Nov. 11–15, Orlando, FL, U.S.. ANS.
Beck, F.R., Jin, Y., Mohanta, L., Qiao, S., Rau, A., Miller, D.J., Cheung, F.B., Lowery, B.R., Bajorek, S.M., Tien, K., Hoxie, C.L., 2016. Effects of period and flow rate on liquid entrainment and the droplet field under forced oscillatory reflood conditions. 17th International Topical Meeting on Nuclear Reactor Thermal Hydraulics, NURETH 2017.
Benjamin, T.B., Ursell, F., 1954. The stability of the plane free surface of a liquid in vertical periodic motion. In: Proceedings of the Royal Society of London A: Mathematical, Physical and Engineering Sciences, 225. The Royal Society, pp. 505–515.
Bestion, D., 2004. Recent Advances in Thermal Hydraulics Modeling for the CATHARE code. Technical Report.
Cheung, F.-B., Mohanta, L., Riley, M.P., 2014. RBHT Reflood Data Evaluation Report: Internal Report. USNRC.
Coddington, E.A., Levinson, N., 1955. Theory of Ordinary Differential Equations. Tata McGraw-Hill Education.
Drazin, P.G., Reid, W.H., 2004. Hydrodynamic Stability. Cambridge University Press.
Faraday, M., 1837. On a peculiar class of acoustical figures; and on certain forms assumed by groups of particles upon vibrating elastic surfaces. In: Abstracts of the Papers Printed in the Philosophical Transactions of the Royal Society of London. The Royal Society London, pp. 49–51.
Funada, T., Joseph, D., 2001. Viscous potential flow analysis of Kelvin–Helmholtz instability in a channel. J. Fluid Mech. 445, 263–283.
Harvey, A., Mackley, M., Stonestreet, P., 2001. Operation and optimization of an oscillatory flow continuous reactor. Ind. Eng. Chem. Res. 40 (23), 5371–5377.
Kelly, R., 1965. The stability of an unsteady Kelvin–Helmholtz flow. J. Fluid Mech. 22 (3), 547–560.
Kumar, K., 1996. Linear theory of faraday instability in viscous liquids. Proc. R. Soc. Lond. Ser. A 452 (1948), 1113–1126.
Kumar, K., Tuckerman, L.S., 1994. Parametric instability of the interface between two fluids. J. Fluid Mech. 279, 49–68.
Lowe, R.J., Koseff, J.R., Monismith, S.G., 2005. Oscillatory flow through submerged canopies: 1. Velocity structure. J. of Geophys. Res. 110 (C10), 1–17.
Maksymov, I.S., Pototsky, A., 2019. Harmonic and subharmonic waves on the surface of a vibrated liquid drop. Phys. Rev. E 100 (5), 053106.
Mohanta, L., Cheung, F.-B., Bajorek, S.M., 2016. Stability of coaxial jets confined in a tube with heat and mass transfer. Phys. A 443, 333–346.
Nayak, A., Chakraborty, B., 1984. Kelvin–Helmholtz stability with mass and heat transfer. Phys. Fluids (1958–1988) 27 (8), 1937–1941.
Nayfeh, A.H., Mook, D.T., 2008. Nonlinear Oscillations. John Wiley & Sons.
Oh, S., Banerjee, S., Yadigaroglu, G., 1986. Reflooding with steady and oscillatory injection: part II: quench front and liquid carryover behavior. J. Heat Transf. 108 (3), 448–456.
Panton, R.L., 2013. Incompressible Flow. John Wiley & Sons.
Pitari, G., Di Genova, G., Mancini, E., Visioni, D., Gandolfi, I., Cionni, I., 2016. Stratospheric aerosols from major volcanic eruptions: a composition-climate model study of the aerosol cloud dispersal and e-folding time. Atmosphere 7 (6), 75.
Pucci, G., 2015. Faraday instability in floating drops out of equilibrium: motion and self-propulsion from wave radiation stress. Int. J. Nonlinear Mech. 75, 107–114.
Rainey, R., 2007. Weak or strong nonlinearity: the vital issue. J. Eng. Math. 58 (1-4), 229–249.
Razavi, H., Gupta, R., Adams, F.C., Bloch, A.M., 2016. Stability of a class of coupled Hill's equations and the Lorentz oscillator model. SIAM J. Appl. Dyn. Syst. 15 (2), 1104–1123.
Rumfeldt, J.A., Galvagnion, C., Vassall, K.A., Meiering, E.M., 2008. Conformational stability and folding mechanisms of dimeric proteins. Prog. Biophys. Mol. Biol. 98 (1), 61–84.
Sleath, J., 1987. Turbulent oscillatory flow over rough beds. J. Fluid Mech. 182, 369–409.
Stokes, G. G., 1880. On the theory of oscillatory waves. Transactions of the Cambridge Philosophical Society.
Stone, P.H., 1972. A simplified radiative-dynamical model for the static stability of rotating atmospheres. J. Atmos. Sci. 29 (3), 405–418.
Watson, E., 1983. Diffusion in oscillatory pipe flow. J. Fluid Mech. 133, 233–244.
Zhou, C., Xie, F., Li, Z., 2020. Complex bursting patterns and fast-slow analysis in a smallest chemical reaction system with two slow parametric excitations. Chaos Solitons Fractals 137, 109859.

Henderson is grateful for support from the National Science Foundation, NSF-DMS-1716159. Beck wishes to acknowledge Partha